


Article

Optimizing Thermal Efficiencies of Double-Pass Cross-Corrugated Solar Air Heaters on Various Configurations with External Recycling

Chii-Dong Ho *, Hsuan Chang, Ching-Fang Hsiao and Yu-Chen Lin

Department of Chemical and Materials Engineering, Tamkang University, Tamsui, New Taipei 251, Taiwan; nhchang@mail.tku.edu.tw (H.C.); tvxqdbkskshw8938@gmail.com (C.-F.H.); julie000222333@gmail.com (Y.-C.L.)

* Correspondence: cdho@mail.tku.edu.tw; Tel.: +886-2-26215656 (ext. 2724); Fax: +886-2-26209887

Abstract: The effect of external-recycle operations on the thermal performance of double-pass cross-corrugated solar air heaters (SAH) under different operating conditions was investigated experimentally and theoretically. Additionally, the simultaneous ordinary equations were solved analytically for each proposed configuration. Four recycling types are introduced for improving the solar thermal performance with different external recycle processes, which are expected to enhance the heat transfer coefficient with a convective turbulent flow between the air and the absorber in the present study. Using recycling double-pass operations, two processes were conducted sequentially: air first flowed over the sinusoidal corrugated absorber plate and then flowed back later over the transverse sinusoidal corrugated bottom plate. Improved device performance was achieved due to the doubled heat transfer area over and under the corrugated absorber plate, from which both the sinusoidal cross-corrugated absorber plate and bottom plate enhanced turbulent intensity. Theoretical predictions and experimental results both indicated that the recycle ratio increased with the SAH thermal efficiency for all proposed designs. The results show a higher heat transfer efficiency for the proposed four configurations using wavelike corrugated plates compared to those conducted in single-pass and flat-plate absorber plates with up to a maximum 133% (from 0.301 to 0.703) increment. The optimal device performance was examined for all external-recycle configurations under the same working dimensions and operational conditions. The best configuration for optimal thermal performance was the device that lengthened the air flow pathway and increased the air velocity within the collector; thus, a higher heat transfer rate was accomplished. The evaluation of increments in the power consumption and of the heat-transfer efficiency enhancement together determined the optimal design based on an economic consideration across various configurations of cross-corrugated double-pass devices.

Keywords: collector thermal efficiency; double-pass operation; solar air collector; external recycle; cross-corrugated module



Citation: Ho, C.-D.; Chang, H.; Hsiao, C.-F.; Lin, Y.-C. Optimizing Thermal Efficiencies of Double-Pass Cross-Corrugated Solar Air Heaters on Various Configurations with External Recycling. *Energies* **2021**, *14*, 4019. <https://doi.org/10.3390/en14134019>

Academic Editor: Carlo Renno

Received: 10 June 2021

Accepted: 30 June 2021

Published: 3 July 2021

Publisher's Note: MDPI stays neutral with regard to jurisdictional claims in published maps and institutional affiliations.



Copyright: © 2021 by the authors. Licensee MDPI, Basel, Switzerland. This article is an open access article distributed under the terms and conditions of the Creative Commons Attribution (CC BY) license (<https://creativecommons.org/licenses/by/4.0/>).

1. Introduction

Solar energy is becoming more available and favorable [1] among many new energy options used by human beings. Solar collectors may be the simplest type of the heat exchanger, which act as a blackbody for receiving worldwide sources of distant solar radiation to convert solar energy over an absorber plate into thermal energy; they have been used widely in many countries to warm water or air [2]. The simplest designs of the flat-plate solar collector for transforming the form of energy are widely implemented in space heating [3], food dehydration and the drying of crops [4], and industrial technologies [5]. Many improved devices have taken design parameters into account. Razika et al. [6] and Al-Kayiem and Yassen [7] discussed the inclination angle for the absorption–convection heat transfer mechanism. Das et al. [8] and El-Sebaei and Al-Snani [9] investigated the effects of using absorber plates coated with various selective coating materials on the

collector performance. Vaziri et al. [10] presented the collector thermal performances of perforated glazed solar air heaters with different inner collector colors. Fudholi et al. [11] and Gupta and Kaushik [12] developed the potential improvement of a solar collector based on energy and exergy analyses.

The main issues of using conventional solar collectors are low convective heat-transfer coefficients due to a viscous laminar sub-layer in the turbulent boundary layer nearby the absorber plate surface as well as the constrained heat-transfer area owing to the economic viewpoint of the capital cost. Turbulence promoters have the potential to overcome these two restrictions, and should be realized by demolishing the laminar sub-layer to create effective momentum exchange and enlarging the heat transfer area to increase the thermal performance. Configurations of design principles attain augmented heat transfer characteristics [13,14] by using different techniques to obtain a higher turbulent intensity, as documented extensively in the literature, such as an extended heat-transfer area using v-groove flow channels [15], various fin shapes [16], thin ribs [17] and baffles [18], and the destroyed laminar sub-layer using flow turbulence with vortex generators [19,20], surface roughening on the absorber plate [21], packing wire mesh [22] and porous medium materials [23], and recycling operations [24].

An alternative approach may be able to enhance the collector thermal efficiency using corrugated/grooved absorber surfaces [25,26] under double passing [27,28] to heat the air twice in flowing channels before exiting the collector. Naphon et al. [29] and Qin et al. [30] explored the heat transfer rate and pressure drop in V-type corrugated channels. Moreover, a corrugated absorber surface has been demonstrated to extract more thermal heat from solar collectors [31], although the power required at the expense of the power consumption due to increases in friction loss also increased. Optimizing the collector thermal performance in double-pass solar air collectors is achieved by operating various flow configurations of different external-recycle types in more efficient designs of thermal energy systems. External recycling with air recirculation operating at simultaneous concurrent- and countercurrent-flow streams produces remixing effects and increases the fluid velocity. Thus, a higher convective heat-transfer coefficient is obtained, comparable to that of the single-pass operation, although accompanied by some undesirable defects [32].

Four recycle-type designs proposed for comparisons in the present study include both advantageous effects in promoting the turbulent intensity enhancement within cross-corrugated solar air collectors and in operating double-pass devices with external recycling. It is believed that assessing the availability of such comparisons presented here for recycling operations in cross-corrugated solar air collectors is the value of this work. It will contribute to designing and examining the economic meaning of solar air collectors when considering both heat-transfer efficiency improvements and power consumption increments. The purpose of the present study is to develop the optimal design experimentally and theoretically and identify the best operational conditions such as the recycle ratio and air mass flow rate. The corrugated absorber configurations investigated in our previous study [33] showed that a significant enhancement of the thermal performance of solar air collectors was achieved. This motivated us to introduce various external-recycle operations to resolve the disadvantages of remixing effects and preserve the advantages of convective turbulent flows in the conventional flat-plate solar air heater upgraded through examining various configurations and operating conditions. The experimental results and theoretical predictions provide an economic evaluation of the technical feasibility to support the appropriate selection of its practical application.

2. The Flow Configurations and Theoretical Formulations

The new recycling double-pass solar air heater design uses a sinusoidal corrugated absorber plate to divide the air flowing conduit into two channels (above and below the wavelike absorber plate) and weld a sinusoidal corrugated bottom plate of the lower channel as well, as illustrated by the schematic side view in Figure 1 for the recycling double-pass solar air collector. The various flow configurations with external recycling

is obvious, and this can be significantly beneficial for absorbing solar heat due to the convective heat-transfer coefficient enlargement on the absorber surface to the air. However, the flow types of various external recycles can be modified to examine the turbulent intensity on the absorber plate as well as the Nusselt number. In the present study, various external-recycle configurations for comparisons are presented, designed to evaluate the heat transfer efficiency.

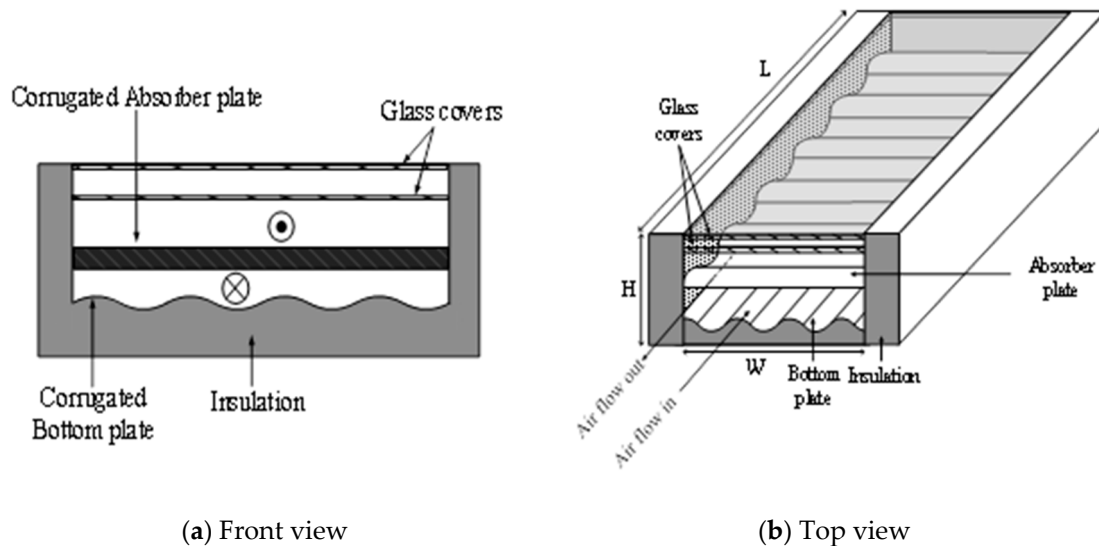


Figure 1. A schematic drawing of a recycling double-pass cross-corrugated solar air heater.

Type A: Internal recycling at the upper channel

A collector of 30 cm long, 30 cm wide with 5 cm and 3.9 cm in height is considered, which is divided into an open conduit by inserting a sinusoidal corrugated absorber plate of negligible thickness and thermal resistance. As an illustration of Type A in Figure 2, prior to entering the lower channel for the second time, the fluid with air mass flow rate \dot{m} and temperature T_i is well mixed with the fluid exiting from the upper channel by the air mass flow rate of recycling $R\dot{m}$ and $T_{b,0}$, directed to the upper channel, which is controlled by means of an appropriate pump situated at the beginning of the lower channel. The purpose of this recycling loop is to heat the air flowing twice through the channels of the solar air collector, and thus, the double-pass operation is then repeated. Various external-recycle types designed in this study, with a Type A schematic presented in Figure 2.

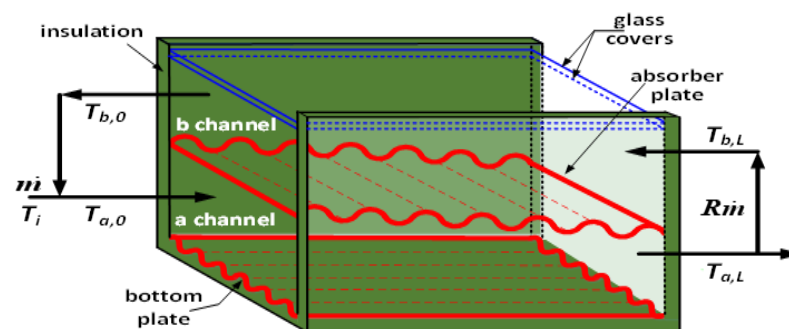


Figure 2. Schematic drawing of a recycling double-pass cross-corrugated solar air heater (Type A).

Balancing energy with the energy-flow diagram present for a finite fluid element of the absorber plate, the glass cover, the bottom plate, and the air flowing into both channels is demonstrated in Figure 3. All the coefficients for various heat-transfer parts of the solar air

heater are consolidated in the thermal resistance network. By following the same procedure performed in our previous work [33] and rearranging with $\xi = z/L$, one obtains

$$\frac{d(T_b(\xi) - T_s)}{d\xi} = B_1[T_b(\xi) - T_s] + B_2[T_a(\xi) - T_s] + B_3 \tag{1}$$

$$\frac{d(T_a(\xi) - T_s)}{d\xi} = B_4[T_b(\xi) - T_s] + B_5[T_a(\xi) - T_s] + B_6 \tag{2}$$

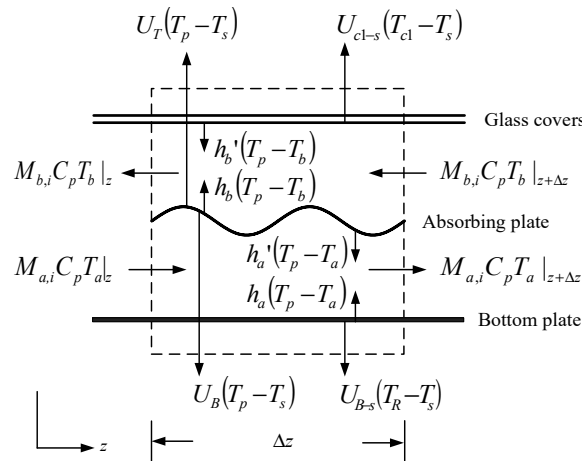


Figure 3. The energy balance achieved within a finite fluid element.

Solar air collectors are different from common heat exchangers, in that the solar radiant energy is transferred from the top side of the device. Therefore, the two side-wall boundaries are adiabatic. The width, which is of the same order as the length of the collector, is relatively large in dimension; therefore, the effects of the two side-wall boundaries are not significant. These considerations lead to the assumption of negligible end effects from the two side walls. The same assumption was taken into account by Duffie and Beckman [34]. The analytical solutions of the temperature distributions in the flowing direction to this recycling double-pass device of Type A were obtained by transforming Equations (1) and (2) into a pair of differential operator equations with the use of the following boundary conditions:

$$\xi = 1, T_a(1) = T_{a,L} \quad T_b(1) = T_{b,L} \quad \text{and} \quad T_{a,L} = T_{b,L} \tag{3}$$

$$\xi = 0, T_a(0) = T_{a,0} = \frac{T_i + RT_b(0)}{1 + R} \tag{4}$$

Temperature distributions were solved by substituting the boundary conditions, Equations (3) and (4), into Equations (1) and (2), and producing Equations (5) and (6) for two channels, respectively. The solutions of temperature distributions were associated with the two distinct roots, Y_1 and Y_2 , of two simultaneous linear ordinary differential equations. There were two undetermined coefficients, C_1 and C_2 , which was also the case when following the same mathematical treatment performed previously [33]:

$$T_a(\xi) = C_1 e^{Y_1 \xi} + C_2 e^{Y_2 \xi} + \frac{B_3 B_4 - B_1 B_6}{B_1 B_5 - B_2 B_4} + T_s \tag{5}$$

$$T_b(\xi) = \frac{Y_1 - B_5}{B_4} C_1 e^{Y_1 \xi} + \frac{Y_2 - B_5}{B_4} C_2 e^{Y_2 \xi} + \frac{B_2 B_6 - B_3 B_5}{B_1 B_5 - B_2 B_4} + T_s \tag{6}$$

$$Y_1 = \left[(B_1 + B_5) + \sqrt{(B_1 - B_5)^2 + 4B_2 B_4} \right] / 2 \tag{7}$$

$$Y_2 = \left[(B_1 + B_5) - \sqrt{(B_1 - B_5)^2 + 4B_2B_4} \right] / 2 \quad (8)$$

$$C_1 = \frac{B_4 (F_2 - F_3)(RI_2 - RI_2e^{Y_2} - B_4) - F_2I_2e^{Y_2}}{F_1 I_1I_2R(e^{Y_1} - e^{Y_2}) - B_4(I_1e^{Y_1} - I_2e^{Y_2})} \quad (9)$$

$$C_2 = \frac{B_4 (F_2 - F_3)(B_4 + RI_1e^{Y_1} - I_1R) + F_2I_1e^{Y_1}}{F_1 I_1I_2R(e^{Y_1} - e^{Y_2}) - B_4(I_1e^{Y_1} - I_2e^{Y_2})} \quad (10)$$

in which:

$$F_1 = B_1B_5 - B_2B_4, F_2 = B_3B_4 - B_1B_6 \text{ and } F_3 = B_2B_6 - B_3B_5 \quad (11)$$

$$I_1 = Y_1 - B_4 - B_5 \text{ and } I_2 = Y_2 - B_4 - B_5 \quad (12)$$

Detailed derivations of these two simultaneous system equations with all the coefficients B_i , G_i , Y_i and C_i are expressed with the convective heat-transfer coefficients, loss coefficients, and physical properties in Figure 2 for Type A as follows:

$$B_1 = \frac{h_b G_1 + h'_b h_{r,p-c1} G_1 G_4 + h'_b G_4 U_{c1-s}}{M_{b,A} / A_c} \quad (13)$$

$$B_2 = \frac{h_b G_2 + h'_b h_{r,p-c1} G_2 G_4}{M_{b,A} / A_c} \quad (14)$$

$$B_3 = \frac{h_b G_3 + h'_b h_{r,p-c1} G_3 G_4}{M_{b,A} / A_c} \quad (15)$$

$$B_4 = \frac{h_a G_6 + h'_a h_{r,p-R} G_6 G_7}{M_{a,A} / A_c} \quad (16)$$

$$B_5 = \frac{h_a G_5 + h'_a h_{r,p-R} G_5 G_7 - h_a G_7 U_{B-s}}{M_{a,A} / A_c} \quad (17)$$

$$B_6 = \frac{h_a G_3 + h'_a h_{r,p-R} G_3 G_7}{M_{a,A} / A_c} \quad (18)$$

$$G_1 = -(h_a + U_T + U_B) / (h_a + h_b + U_T + U_B) \quad (19)$$

$$G_2 = h_a / (h_a + h_b + U_T + U_B) \quad (20)$$

$$G_3 = I_0 \alpha_p \tau_g^2 / (h_a + h_b + U_T + U_B) \quad (21)$$

$$G_4 = (h'_b + h_{r,p-c1} + U_{c1-s})^{-1} \quad (22)$$

$$G_5 = -(h_b + U_T + U_B) / (h_a + h_b + U_T + U_B) \quad (23)$$

$$G_6 = h_b / (h_a + h_b + U_T + U_B) \quad (24)$$

$$G_7 = (h'_a + h_{r,p-R} + U_{B-s})^{-1} \quad (25)$$

in which the radiation through both the inner cover and outer cover to the ambient air with heat transfer coefficients in all the constants B_i , G_i , Y_i and C_i are calculated by empirical expressions [34,35]:

$$U_T = \left\{ \frac{(T_{p,m}/520)}{\left[\frac{(T_{p,m}-T_0)}{2+(1+0.089h_w-0.1166h_w\varepsilon_p)(1+0.07866 \times 2)} \right]^{0.43(1-100/T_{p,m})} + \frac{1}{h_w}} \right\}^{-1} \quad (26)$$

$$+ \frac{\sigma(T_{p,m}+T_0)(T_{p,m}^2+T_0^2)}{(\varepsilon_p+1 \times 0.00591h_w)^{-1} + [2 \times 2 + (1+0.089h_w-0.1166h_w\varepsilon_p)(1+0.07866 \times 2) - 1 + 0.133\varepsilon_p] / \varepsilon_g - 2}$$

$$\frac{1}{U_{c1-s}} = \frac{1}{h_w + h_{r,c2-s}} + \frac{1}{h_{c1-c2} + h_{r,c1-c2}} = \frac{1}{(2.8+3.0V) + \epsilon_g \sigma (T_{c2,m}^2 + T_0^2)(T_{c2,m} + T_0)} + \frac{1}{1.25(T_{c1,m} - T_{c2,m})^{0.25} + \frac{\sigma(T_{c1,m}^2 + T_{c2,m}^2)(T_{c1,m} + T_{c2,m})}{(1/\epsilon_g) + (1/\epsilon_g) - 1}} \quad (27)$$

The forced convective heat-transfer coefficient between two cross-corrugated plates is required to analyze the heat transfer characteristics of the solar air collector and collector-storage walls. The average Nusselt number is an important non-dimensional parameter, and is determined for the lower channel by the following correlation [36] for the cross-corrugated collector:

$$Nu_a = \frac{h_a De_a}{k} = 0.0743 Re_a^{0.76}, \quad 3000 \leq Re_a \leq 50,000 \quad (28)$$

Similarly, the Nusselt number in the upper channel can be estimated and developed by the following correlation [37] as:

$$Nu_b = \frac{h_b De_b}{k} = 0.1673 (Ra \times \cos\theta)^{0.2917}, \quad Ra = \frac{1}{T_i} \frac{\rho^2 C_p g \beta (T_{pm} - T_{bm}) H_c^3}{k \mu} \quad (29)$$

whereas the equation presented by laminar flow [38] could be used:

$$Nu_0 = 4.4 + \frac{0.00398(0.7 Re_0 De_0 / L)^{1.66}}{1 + 0.0114(0.7 Re_0 De_0 / L)^{1.12}} \quad (30)$$

in which the hydraulic mean diameter denotes the hydraulic diameter of the absorber channel for calculating the Reynolds number, which is expressed in terms of characteristic lengths of the working dimensions in double-pass operations, De_a and De_b , and in single-pass operations, De_0 , respectively:

$$De_a = \frac{2WH_g}{W + H_g}, \quad De_b = \frac{2WH_c}{W + H_c}, \quad De_0 = \frac{2W(H_g + H_c)}{(W + H_g + H_c)} \quad (31)$$

where H_g is the average gap between the absorber plate and the bottom plate, and H_c is the average gap thickness between the inner cover and the absorber plate, and the average velocities of the lower and upper channels and the Reynolds numbers for both channels are:

$$\bar{v}_0 = \frac{\dot{m}}{(H_g + H_c)\rho}, \quad \bar{v}_a = \frac{(1+R)\dot{m}}{H_g\rho}, \quad \bar{v}_b = \frac{R\dot{m}}{H_c\rho} \quad (32)$$

$$Re_0 = \frac{2\dot{m}}{\mu(W + H_g + H_c)}, \quad Re_a = \frac{2\dot{m}(1+R)}{\mu(W + H_g)}, \quad Re_b = \frac{2\dot{m}R}{\mu(W + H_c)} \quad (33)$$

Meanwhile, the collector thermal efficiency $\eta_{C,A}$ of Type A can be combined with the actual useful energy gained by the airflow in both channels and incident solar radiation, and the average absorber plate temperature as well, i.e.,

$$\eta_{C,A} = \frac{Q_u(\text{Useful gain of energy carried away by air})}{I_0 A_c (\text{Total solar radiation incident})} = \frac{\dot{m} C_p (T_{a,L} - T_i)}{A_c I_0} = \alpha_p \tau_g^2 - \frac{U_L (T_{p,m} - T_0)}{I_0} \quad (34)$$

Then, the outlet temperature of $T_{a,L}$ can be calculated from Equation (5) with the use of Equation (3):

$$T_{a,L} = T_a(1) = C_1 e^{Y_1} + C_2 e^{Y_2} - \frac{B_3 B_4 - B_1 B_6}{B_1 B_5 - B_2 B_4} + T_0 \quad (35)$$

The overall heat loss coefficient U_L was estimated by summing the top and bottom loss coefficients U_T and U_B , respectively, and neglecting edge loss then can be expressed as follows:

$$U_L = U_T + U_B \tag{36}$$

The average absorber temperature is thus obtained by equating the terms on the right-hand side of Equation (34):

$$T_{p,m} = T_0 + \left(I_0 \tau_g^2 \alpha_p / U_L \right) - \frac{\dot{m} C_p (T_{a,L} - T_i)}{A_c U_L} = T_0 + (I_0 / U_L) \left(\tau_g^2 \alpha_p - \eta_{C,A} \right) \tag{37}$$

The collector efficiency improvements, i.e., I_d and $I_{C,A}$, are evaluated by defining the percentage of the improvement within the collector efficiency of the double-pass flat-plate device and the present recycling double-pass cross-corrugated device (as compared to the downward-type single-pass device) under the same working dimensions as

$$I_d = \frac{\text{collector efficiency of flat-plate double-pass device, } \eta_d}{\text{collector efficiency of downward single-pass device, } \eta_s} - 1 \tag{38}$$

$$I_{C,A} = \frac{\text{collector efficiency of double-pass cross-corrugated device, } \eta_{C,A}}{\text{collector efficiency of downward single-pass device, } \eta_s} - 1 \tag{39}$$

in which η_d , $\eta_{C,A}$ and η_s denote collector efficiencies of the double-pass flat-plate, double-pass cross-corrugated and downward-type single-pass devices, respectively.

Further collector efficiency enhancement $E_{C,A}$ in collector efficiency by inserting the corrugated absorber plate in the flow channel is calculated based on the device of the flat-plate absorber:

$$E_{C,A} = \frac{\eta_{C,A} - \eta_d}{\eta_d} = \left[\frac{(\eta_{C,A} - \eta_s) - (\eta_d - \eta_s)}{\eta_s} \right] (\eta_s / \eta_d) = (I_{C,A} - I_d) (\eta_s / \eta_d) = \frac{I_{C,A} - I_d}{1 + I_d} \tag{40}$$

Type A and other external-recycle configurations are demonstrated and explained using the boundary condition and air mass flow rate, as summarized in Table 1, and the theoretical predictions of the collector thermal efficiency and outlet temperature are developed and listed in Table 2. Hereafter, the external-recycle types delineated in Figures 4–6 are labelled Types B, C and D, correspondingly. Similarly, two undetermined coefficients, C_1 and C_2 , in Equations (5) and (6) were solved and are shown in Table 3.

Table 1. Air mass flow rates and boundary conditions for Type A–D.

Flow Type	Lower Channel $M_{a,i}$	Upper Channel $M_{b,i}$	Boundary Condition, $\zeta=0$	Boundary Condition, $\zeta=1$
A	$\dot{m}(1 + R)$	$\dot{m} R$	$T_a(0) = T_{a,0} = \frac{T_i + RT_b(0)}{1+R}$	$T_a(1) = T_{a,L} = T_b(1) = T_{b,L}$
B	$\dot{m}(1 + R)$	\dot{m}	$T_a(0) = T_{a,0} = \frac{T_i + RT_a(1)}{1+R}$	$T_a(1) = T_{a,L} = T_b(1) = T_{b,L}$
C	\dot{m}	$\dot{m}(1 + R)$	$T_a(0) = T_i$	$T_b(1) = T_{b,L} = \frac{T_{a,L} + RT_b(0)}{1+R}$
D	$\dot{m}(1 + R)$	$\dot{m}(1 + R)$	$T_a(0) = \frac{T_i + RT_b(0)}{1+R}$	$T_a(1) = T_{a,L} = T_b(1) = T_{b,L}$

Table 2. Theoretical predictions of the collector thermal efficiency and outlet temperature for all flow types.

Flow Type	Collector Thermal Efficiency	Outlet Temperature
A	$\eta_{C,A} = \frac{\dot{m} C_p (T_{a,L} - T_i)}{A_c I_0} = \alpha_p \tau_g^2 - \frac{U_L (T_{p,m} - T_s)}{I_0}$	$T_{a,L} = T_a(1) = C_1 e^{Y_1} + C_2 e^{Y_2} - \frac{B_3 B_4 - B_1 B_6}{B_1 B_5 - B_2 B_4} + T_s$
B	$\eta_{C,B} = \frac{\dot{m} C_p (T_{b,0} - T_i)}{A_c I_0}$	$T_{b,0} = T_b(0) = C_1 e^{Y_1} + C_2 e^{Y_2} - \frac{B_3 B_4 - B_1 B_6}{B_1 B_5 - B_2 B_4} + T_s$
C	$\eta_{C,C} = \frac{\dot{m} C_p (T_{b,0} - T_i)}{A_c I_0}$	$T_b(1) = T_{b,L} = \frac{T_{a,L} + RT_b(0)}{1+R}$
D	$\eta_{C,D} = \frac{\dot{m} C_p (T_{b,0} - T_i)}{A_c I_0}$	$T_a(1) = T_{a,L} = T_b(1) = T_{b,L}$

Table 3. Two undetermined coefficients, C_1 and C_2 , in Equations (5) and (6) for all flow types.

Flow Type	C_1	C_2
A	$C_1 = \frac{B_4 (F_2 - F_3) (R I_2 - R I_2 e^{\gamma_2} - B_4) - F_2 I_2 e^{\gamma_2}}{F_1 I_1 I_2 R (e^{\gamma_1} - e^{\gamma_2}) - B_4 (I_1 e^{\gamma_1} - I_2 e^{\gamma_2})}$	$C_2 = \frac{B_4 (F_2 - F_3) (B_4 + R I_1 e^{\gamma_1} - I_1 R) + F_2 I_1 e^{\gamma_1}}{F_1 I_1 I_2 R (e^{\gamma_1} - e^{\gamma_2}) - B_4 (I_1 e^{\gamma_1} - I_2 e^{\gamma_2})}$
B	$C_1 = \frac{1}{F_1} \frac{I_2 F_2 e^{\gamma_2} + B_4 (F_2 - F_3) (1 + R - R e^{\gamma_2})}{(I_1 e^{\gamma_1} - I_2 e^{\gamma_2}) (1 + R) - (I_1 - I_2) e^{\gamma_1} e^{\gamma_2} R}$	$C_2 = -\frac{1}{F_1} \frac{I_1 F_2 e^{\gamma_1} + B_4 (F_3 - F_2) (1 + R - R e^{\gamma_1})}{(I_1 e^{\gamma_1} - I_2 e^{\gamma_2}) (1 + R) - (I_1 - I_2) e^{\gamma_1} e^{\gamma_2} R}$
C	$C_1 = \frac{1}{F_1} \frac{B_4 (F_2 - F_3) + F_2 e^{\gamma_2} (I_2 + H_2 R) - F_2 H_2 R}{e^{\gamma_1} (I_1 + H_1 R) - e^{\gamma_2} (I_2 + H_2 R) - R (H_1 - H_2)}$ $H_1 = Y_1 - B_5, H_2 = Y_2 - B_5$	$C_2 = -\frac{1}{F_1} \times \frac{B_4 (F_2 - F_3) + F_2 e^{\gamma_1} (I_1 + H_1 R) - F_2 H_1 R}{e^{\gamma_1} (I_1 + H_1 R) - e^{\gamma_2} (I_2 + H_2 R) - R (H_1 - H_2)}$ $H_1 = Y_1 - B_5, H_2 = Y_2 - B_5$
D	$C_1 = \frac{B_4 (F_3 - F_2) (R I_2 e^{\gamma_2} + B_4 - R I_2) - F_2 I_2 e^{\gamma_2}}{F_1 I_2 e^{\gamma_2} (B_4 - R I_1) - I_1 e^{\gamma_1} (B_4 - R I_2)}$	$C_2 = \frac{B_4 (F_2 - F_3) (R I_1 e^{\gamma_1} + B_4 - R I_1) - F_2 I_1 e^{\gamma_1}}{F_1 I_2 e^{\gamma_2} (B_4 - R I_1) - I_1 e^{\gamma_1} (B_4 - R I_2)}$

Type B: External recycling at the lower channel

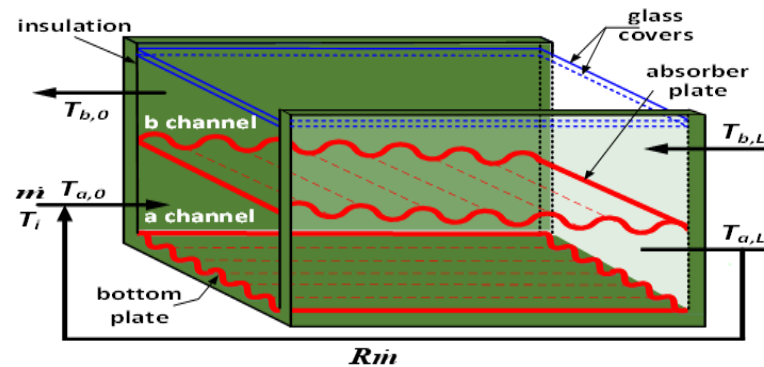


Figure 4. Schematic drawing of a recycling double-pass cross-corrugated solar air heater (Type B).

Type C: External recycling at the upper channel

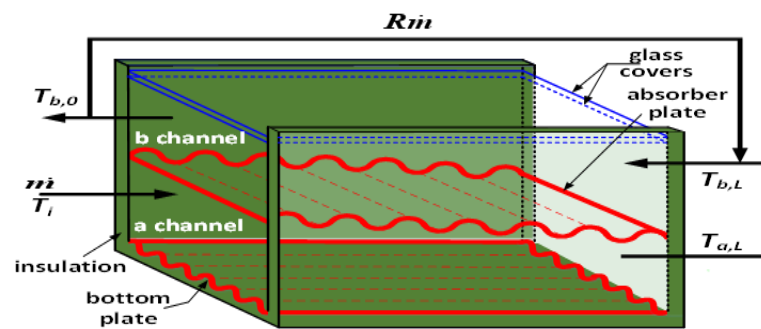


Figure 5. Schematic drawing of a recycling double-pass cross-corrugated solar air heater (Type C).

Type D: Equal recycling of both channels

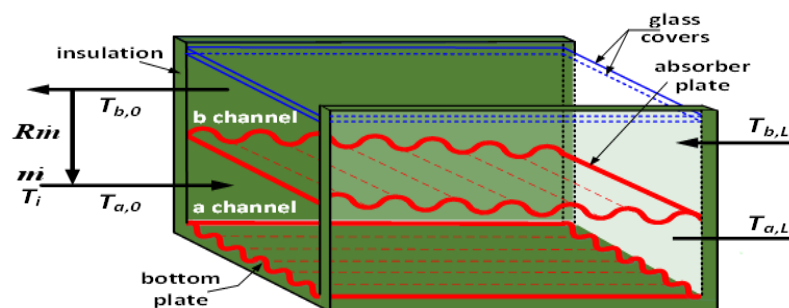


Figure 6. Schematic drawing of a recycling double-pass cross-corrugated solar air heater (Type D).

Furthermore, the Fanning friction factor of the recycling cross-corrugated solar air collector would be increased due to the intensive turbulence and the recycle-effect operation. The degree of power consumption for the flat-plate, cross-corrugated and single-pass solar air collector are defined as Equations (41)–(43), respectively [39], as follows:

$$f_{F,j} = \frac{24}{Re_i}, \text{ for } Re_j < 2100, j = b, 0 \text{ for flat – plate device} \quad (41)$$

$$f_{F,j} = \frac{0.0791}{Re_i^{0.25}}, \text{ for } 2100 < Re_j < 100,000, j = b, 0 \text{ for flat – plate device} \quad (42)$$

$$f_{F,a} = \frac{6.536}{Re_a^{0.421}}, \text{ for } 3000 < Re_a < 50,000 \text{ for cross – corrugated device} \quad (43)$$

The recycling double-pass operations with implementing cross-corrugated absorber plate and bottom plate are defined as:

$$\ell w_{f,j} = \frac{2f_{F,i}\bar{v}_i^2 L}{De_i}, j = a, b, 0 \quad (44)$$

$$P_{C,i} = M_{a,i}\ell w_{f,a} + M_{b,i}\ell w_{f,b} = M_{a,i}\left(2f_{F,a}\bar{v}_a^2 L/De_a\right) + M_{b,i}\left(2f_{F,b}\bar{v}_b^2 L/De_b\right), i = A, B, C, D \quad (45)$$

which are associated with the hydraulic dissipated energy and the increase in power consumption as compared to the downward single-pass operation $P_s = \dot{m}\ell w_{f,s} = 2f_{F,s}\bar{v}_0^2 L/De_0$. The power consumption increments for the double-pass cross-corrugated and double-pass flat-plate devices are defined as

$$I_{P,i} = \frac{P_{C,i} - P_s}{P_s}, i = A, B, C, D, \text{ for cross – corrugated solar air collectors} \quad (46)$$

$$I_{P,d} = \frac{P_d - P_s}{P_s}, \text{ for double – pass flat – plate solar air collector} \quad (47)$$

3. Experimental Setup and Procedure

The experimental setup was fabricated, and the experimental procedure is approved for experimental runs to establish the validity of the phenomena of the heat transfer problems, where the collector thermal performance was examined for various configurations of recycling double-pass sinusoidal cross-corrugated solar air collectors, as shown in Figures 7–10 to represent four external-recycle types. The experimental measurements provided a set of experimental results to validate the theoretical predictions of cross-corrugated solar air collectors.

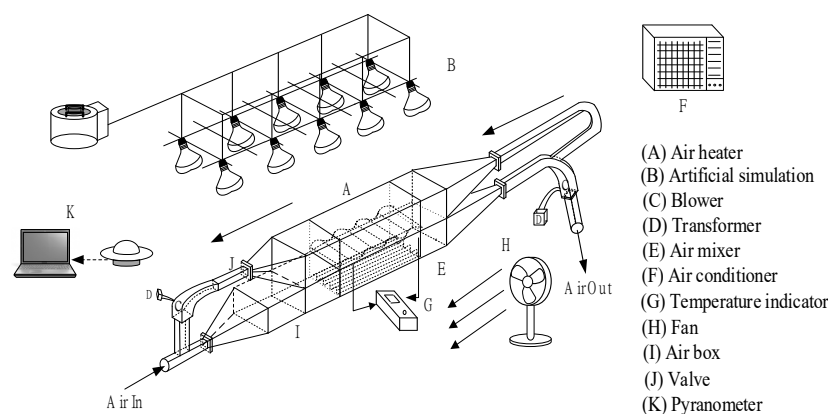


Figure 7. Experimental setup of a recycling cross-corrugated solar air collector (Type A).

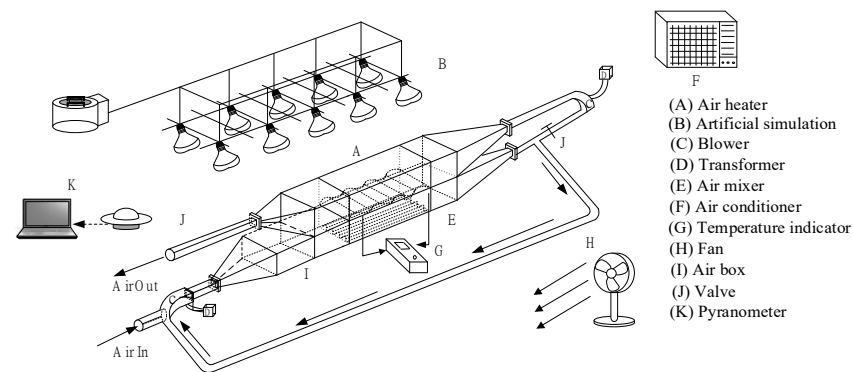


Figure 8. Experimental setup of a recycling cross-corrugated solar air collector (**Type B**).

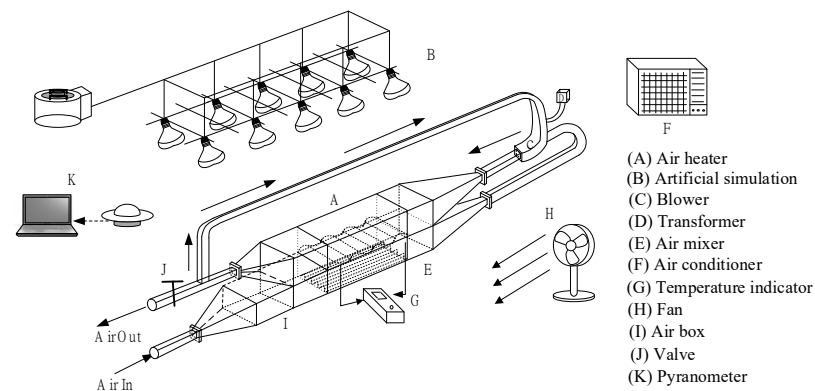


Figure 9. Experimental setup of a recycling cross-corrugated solar air collector (**Type C**).

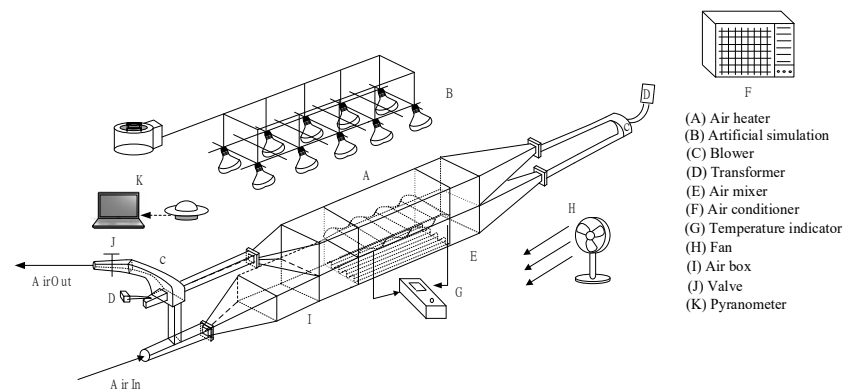


Figure 10. Experimental setup of a recycling cross-corrugated solar air collector (**Type D**).

The experimental setup of the proposed solar air collectors was 30 cm long and 30 cm wide, and the main components of the collectors consisted of two air blowers, two glass covers to reduce the amount of heat loss to the environment, one set of adjustable heat sources, a sinusoidal wavelike absorber plate and a sinusoidal wavelike bottom plate. There was an air box with a preheater, as shown in Figure 11, which was used for air distribution and temperature regulation at the inlet of the main part of the collector, and was designed to diminish the end effects on the velocity profile and offering a developing region in front of the entrance, shown as part (I) in Figures 7–10. A photograph of the present experimental device was taken and is shown in Figure 11. Each external-recycle type has been fabricated using the same main part of the collector, except for rebuilding the connected pipes at both inlet and outlet ends according to the external-recycle configurations in Figures 7–10 to conduct recycling operations.

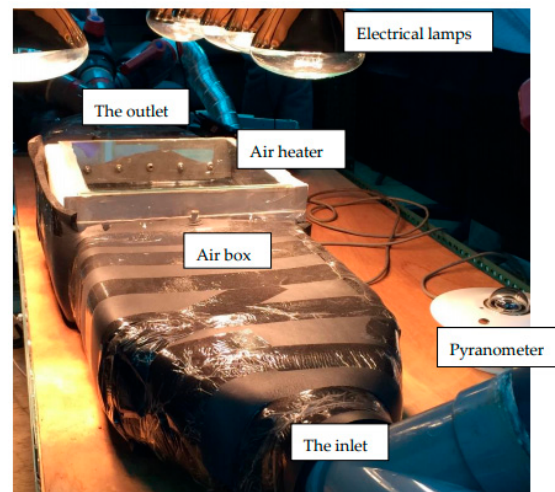


Figure 11. A photo of the external-recycle experimental setup.

To minimize heat losses to the surroundings, the edge and bottom sides of the collector were made of foamed plastic which acted as well-insulated walls. The upper and lower channels of the solar air collectors were fulfilled by inserting a painted black corrugated absorber plate between the lower glass and the sinusoidal wavelike corrugated bottom plate, where average heights of 5 cm and 3.9 cm were created, respectively, and the air flowed simultaneously over and under the absorber plate in a countercurrent direction. Two perforated aluminum plates were placed perpendicular to flowing direction for proper remixing at the inlet and the outlet of ducts. The inlet and outlet temperatures were measured by thermocouples (Type k, 1/4) and then recorded for further calculations (Yokogawa μ R100, Model 4156, Tokyo, Japan). The environment around the solar air collector with a specified convection velocity of 1.0 m/s was measured by using an electrical fan (EUPA TSK-F1426, 14", Tsannkuen Co., Ltd., Taipei, Taiwan). The blower (Teco 3 Phase Induction Motor, Model BL model 552, Redmond Co, Owosso, MI, USA) was used to steadily regulate the air mass flow rate with a control valve, and it was measured with an anemometer (Kanomax Japan Inc., Osaka, Japan). The incident solar radiations were simulated using 14 electrical energy supplies (110 V, 125 W). The electrical lamps used in this experimental setup produced infrared light radiation, and these heating sources and the incident radiation I_0 were measured by using a pyranometer (Model No. 455, Epply Laboratory Inc., Newport, RI, USA). The major influences on both outdoor and indoor test conditions were variations in solar energy or a high temperature difference from sunrise to sunset. These 14 lamps were fixed on a board at a height of 0.16 m above the collector, adjusted using an on/off switch to maintain the specified operating conditions, and the incident radiations were measured on four corners of the main collector box at 10 min intervals.

4. Collector Efficiency Improvement and Further Collector Efficiency Enhancement

The collector efficiency improvement was assessed by calculating the percentage increase in the device performance when employing the recycling double-pass cross-corrugated solar air collector, which was calculated based on the downward-type single-pass device under the same total flow rate \dot{m} and the same working dimensions. The numerical values of the design and operating conditions are as follows: $A_c = 0.09 \text{ m}^2$, $H_g = 0.05 \text{ m}$, $H_c = 0.039 \text{ m}$, $L = 0.3 \text{ m}$, $W = 0.3 \text{ m}$, $\alpha_p = 0.96$, $\varepsilon_g = 0.94$, $\varepsilon_p = 0.8$, $\varepsilon_R = 0.94$, $\tau_g = 0.875$, $k_s = 0.033 \text{ W/m K}$, $\dot{m} = 0.0107$, 0.0161 and 0.0214 kg/s , $T_i = 20 \pm 0.1 \text{ }^\circ\text{C}$, $T_0 = 20 \pm 0.1 \text{ }^\circ\text{C}$, $I_0 = 830 \pm 20$ and $1100 \pm 20 \text{ W/m}^2$, $V = 1.0 \text{ m/s}$. The reason for the two different selections of solar radiation values of $I_0 = 830$ and 1100 W/m^2 was to represent cloudy and sunny days, respectively. Prior to entering the lower channel for the second time, the fluid with temperature T_i is well mixed with the fluid exiting from the upper

channel with the inlet temperature $T_a(0) = T_{a,0} = [T_i + RT_b(0)] / (1 + R)$ for Type A, for example. With $I_0 = 1100 \text{ W/m}^2$ and $T_i = 293 \text{ K}$ for Type A, the temperature change of the air was $6.6 \text{ }^\circ\text{C}$, i.e., $\Delta T = T_b(0) - T_{a,0} = 6.6 \text{ }^\circ\text{C}$ ($49.1 \text{ }^\circ\text{C} - 42.5 \text{ }^\circ\text{C}$). The physical properties of air with this temperature difference were small, for instance, the thermal conductivities of the air were 0.0272 W/mK and 0.0287 W/mK for $40 \text{ }^\circ\text{C}$ and $60 \text{ }^\circ\text{C}$, respectively, according to physical properties of air in the previous study [34]. Therefore, the use of average values of properties and parameters can be justified.

The comparisons have shown improvements in the collector efficiency $I_{C,i}$ ($i = A, B, C, D$) for the double-pass cross-corrugated solar air collector with external-recycle operations. A comparison of the device performance for all external-recycle types in both cross-corrugated and flat-plate solar air collectors is depicted in Table 4. In general, the collector efficiency enhanced by employing the Type C double-pass cross-corrugated solar air collector is more significant than those with other external-recycle types. The theoretical predictions of collector efficiencies under various flow types and recycle ratios are summarized in Table 4 for $I_0 = 1100 \text{ W/m}^2$ and $T_i = 293 \text{ K}$, and the experimental results are based on solar air collectors equipped with a corrugated absorber plate to conduct the validation process. It can also be observed from Table 4 that the order of the device performance of collector efficiencies from employing double-pass cross-corrugated solar air collectors with external recycling is Type C > Type B > Type D > Type A. The external-recycle remixing in the upper channel qualitatively illustrates a higher extent of natural convection on the larger amount of the air mass flow rate of recycle $(R + 1)\dot{m}$ and the exiting temperature $T_{b,0}$, which is directed to the upper channel of Type C. It is important to evaluate the useful energy gained above the corrugated absorber plate in the upper channel; there was a higher exiting temperature from Type C than any other types. As expected, the increase in air mass flow rate and recycle ratio resulted in a greater collector efficiency. Collector efficiencies increased with the air mass flow rate and recycle ratio due to the enlarged flowing air velocity and augmented convective heat-transfer coefficient resulting from employing the cross-corrugated absorber plate and bottom plate. The theoretical predictions and experimental results of the collector thermal efficiencies are presented graphically for comparisons in Figure 12. It is indicated in Figure 12 that the collector efficiency of Type C is higher than those of other types. A larger recycle ratio can substantially integrate heat transfer augmentation of the turbulent intensity into the upper channel of Type C. Type C creates a higher air mass flow rate by remixing the external recycle, in contrast to Type A, to achieve more benefits in enhancing the collector thermal efficiency—by approximately 12% under the same operational conditions. The maximum collector efficiency achieved in the present study is higher than that of flat-plate solar air collectors by about 26% under similar thermal and operating conditions. Overall, implementing the corrugated absorber plate into parallel-plate solar air collectors instead of the flat-plate collector suggests a promising potential to significantly enhance the collector efficiency in the recycling double-pass module. Thus, the increment of turbulent intensity is crucial not only in solar collector engineering designs, but also in other solar thermal technologies.

Moffat [40] determined the error analysis of experimental uncertainty for each individual measurement directly from the experimental results, as follows:

$$S_{\eta_{\text{exp}}} = \left\{ \sum_{i=1}^{N_{\text{exp}}} \frac{(\eta_{\text{exp},i} - \bar{\eta}_{\text{exp},i})^2}{N_{\text{exp}} - 1} \right\}^{1/2} \quad (48)$$

$$S_{\bar{\eta}_{\text{exp}}} = \frac{S_{\eta_{\text{exp}}}}{\sqrt{N_{\text{exp}}}} \quad (49)$$

Table 4. Effects of external-recycle types and recycle ratios on collector efficiency improvements.

$\dot{m}(\text{kg s}^{-1})$	R	Type A			Type B			Type C			Type D		
		$\eta_{C,A}$			$\eta_{C,B}$			$\eta_{C,C}$			$\eta_{C,D}$		
		η_d	Exp.	Theo.	η_d	Exp.	Theo.	η_d	Exp.	Theo.	η_d	Exp.	Theo.
0.0107	0.25	0.374	0.566	0.577	0.430	0.576	0.623	0.444	0.682	0.703	0.394	0.590	0.615
	0.5	0.404	0.585	0.592	0.453	0.585	0.627	0.467	0.687	0.703	0.417	0.594	0.616
	0.75	0.426	0.594	0.603	0.472	0.594	0.630	0.486	0.692	0.703	0.436	0.599	0.617
	1.0	0.443	0.603	0.612	0.488	0.603	0.632	0.502	0.692	0.703	0.452	0.603	0.618
	1.25	0.458	0.613	0.619	0.502	0.613	0.635	0.516	0.693	0.704	0.466	0.608	0.619
0.0161	0.25	0.430	0.587	0.614	0.485	0.643	0.690	0.498	0.727	0.753	0.448	0.636	0.656
	0.5	0.459	0.601	0.628	0.507	0.657	0.694	0.520	0.733	0.753	0.470	0.643	0.657
	0.75	0.479	0.615	0.639	0.525	0.671	0.698	0.538	0.734	0.754	0.488	0.647	0.659
	1.0	0.495	0.622	0.647	0.540	0.685	0.702	0.553	0.740	0.754	0.503	0.650	0.660
	1.25	0.509	0.629	0.654	0.553	0.692	0.705	0.566	0.745	0.754	0.516	0.650	0.661
0.0214	0.25	0.468	0.594	0.633	0.521	0.687	0.742	0.535	0.758	0.781	0.485	0.659	0.678
	0.5	0.495	0.613	0.646	0.542	0.706	0.747	0.556	0.761	0.781	0.506	0.665	0.679
	0.75	0.514	0.631	0.655	0.559	0.724	0.752	0.573	0.767	0.781	0.523	0.668	0.681
	1.0	0.530	0.650	0.663	0.573	0.743	0.756	0.587	0.771	0.781	0.537	0.668	0.682
	1.25	0.542	0.659	0.669	0.585	0.743	0.759	0.599	0.771	0.781	0.548	0.676	0.684

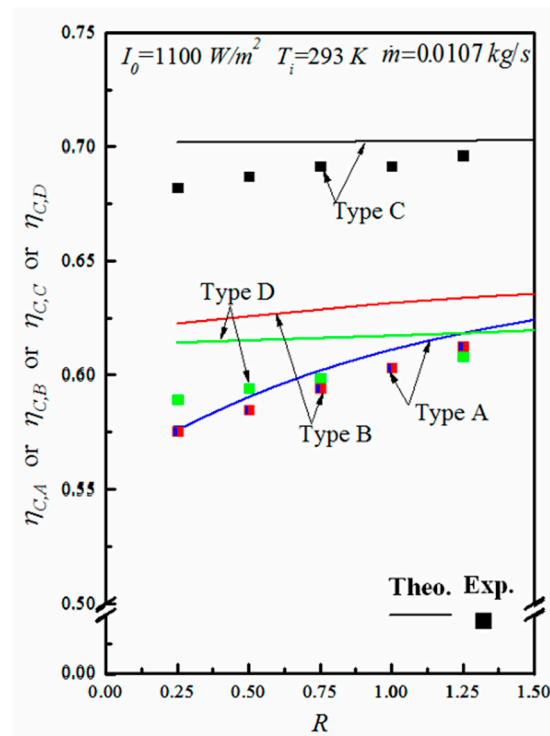


Figure 12. Effect of the recycling ratio on collector efficiency of four types.

The mean experimental uncertainty for $I_0 = 1100 \text{ W/m}^2$ and $T_i = 293 \text{ K}$ of four external-recycle types was calculated. The range of mean experimental uncertainty of the measurements in Table 4 was $5.12 \times 10^{-3} \leq S_{\eta_{\text{exp}}} \leq 9.47 \times 10^{-3}$. Meanwhile, the accuracy deviations of the experimental results from the theoretical predictions were calculated using the following definition:

$$Er = \frac{1}{N_{\text{exp}}} \sum_{i=1}^{N_{\text{exp}}} \frac{|\eta_{\text{theo},i} - \eta_{\text{exp},i}|}{\eta_{\text{theo},i}} \quad (50)$$

where N_{exp} , $\eta_{theo,i}$ and $\eta_{exp,i}$ are the number of experimental runs, theoretical predictions and experimental results of collector efficiencies, respectively. The accuracy deviations with two incident solar radiation are shown in Table 5. The agreement of experimental results deviating from theoretical predictions was quite strong, within $1.01 \times 10^{-2} \leq Er \leq 9.30 \times 10^{-2}$.

Table 5. The accuracy deviation between theoretical predictions and experimental results.

\dot{m} (kg s ⁻¹)	R	$Er \times 100\%$							
		$I_0 = 830 \text{ W/m}^2$				$I_0 = 1100 \text{ W/m}^2$			
		Type A	Type B	Type C	Type D	Type A	Type B	Type C	Type D
0.0107	0.25	2.39	9.02	3.64	4.61	1.82	7.67	2.89	4.15
	0.5	2.69	5.45	2.76	3.75	1.15	6.65	2.24	3.54
	0.75	2.41	3.90	1.88	3.30	1.49	5.62	1.61	2.95
	1.0	1.75	2.33	1.01	3.06	1.42	4.57	1.63	2.36
	1.25	1.85	1.72	1.05	3.23	1.06	3.47	1.01	1.79
0.0161	0.25	5.93	9.30	3.94	2.69	4.45	6.88	3.57	3.14
	0.5	4.93	7.09	3.19	2.00	4.32	5.40	2.66	2.24
	0.75	3.49	4.89	2.70	2.18	3.72	3.92	2.67	1.79
	1.0	3.26	2.67	1.96	1.80	3.89	2.42	1.76	1.56
	1.25	2.78	2.29	1.48	1.16	3.82	1.85	1.22	1.77
0.0214	0.25	7.02	8.30	4.34	1.31	6.15	7.44	2.95	2.77
	0.5	4.85	5.51	3.38	1.49	5.07	5.55	2.48	2.12
	0.75	4.28	4.41	2.74	1.31	3.63	3.65	1.77	1.77
	1.0	3.45	3.27	1.78	1.15	1.93	1.72	1.31	1.97
	1.25	2.42	2.05	1.14	1.01	1.44	2.17	1.32	1.11

The theoretical collector efficiency improvements and further collector efficiency enhancements by employing cross-corrugated double-pass solar air collectors for various external-recycle types and incident radiations are summarized in Tables 6 and 7 for $I_0 = 830 \text{ W/m}^2$ and $I_0 = 1100 \text{ W/m}^2$ with $T_i = 293 \text{ K}$, respectively. The highest collector efficiency improvements achieved were up to 121% and 133% with $T_i = 293 \text{ K}$ for $I_0 = 830$ and $I_0 = 1100 \text{ W/m}^2$ when operating with Type C. The collector efficiency improvement $I_{C,C} = 133.44\%$ improvement (in which $\eta_s = 0.301$ and $\eta_{C,C} = 0.70264$) was achieved when employing the Type C cross-corrugated double-pass solar air rather than the same flat-plate device under $I_0 = 1100 \text{ W/m}^2$, $T_i = 293 \text{ K}$, $\dot{m} = 0.0107 \text{ kg/s}$ and $R = 0.25$, as illustrated in Table 7. Further collector efficiency enhancements are expected if there are two corrugated plates welded and cross-directed in parallel into a flat-plate conduit to increase the turbulent intensity enlargement, in which the convective heat-transfer coefficient increment is acquired. Further collector efficiency enhancement of the device with a welded cross-corrugated absorber plate and bottom plate increases with the air mass flow rate, but decreases with the incident solar radiation and recycle ratio, as displayed in Tables 6 and 7. A higher enhancement, of about a 540% increase in collector efficiency, was observed at the lower recycle ratio and smaller incident solar radiation. The index factor of the improvement in augmented passive heat transfer devices—defined as the value of the Nusselt number for the cross-corrugated case divided by that of its friction factor over the value of the Nusselt number divided by that of the friction factor for the base case, the ratio $[Nu_a/f_{F,a}]/[Nu_0/f_{F,0}] \cong 2.58$ for Type A with $\dot{m} = 0.0214 \text{ kg/s}$ and $R = 1$ —was calculated in the present study as an illustration. It was decided that the strategy used in the present design for heat transfer augmentation was worthwhile when the ratio was greater than one.

Table 6. Theoretical predictions of collector efficiency improvements and further collector efficiency enhancements with $I_0 = 830 \text{ W/m}^2$.

$\dot{m}(\text{kg s}^{-1})$	R	Type A		Type B		Type C		Type D	
		$I_{C,A}$	$E_{C,A}$	$I_{C,B}$	$E_{C,B}$	$I_{C,C}$	$E_{C,C}$	$I_{C,D}$	$E_{C,D}$
0.0107	0.25	79.49	261.62	96.95	357.95	121.08	470.76	96.19	354.40
	0.5	84.12	156.02	97.93	218.13	121.11	292.68	96.49	213.51
	0.75	87.68	116.65	98.88	161.34	121.16	219.65	96.81	155.94
	1.0	90.47	93.10	99.76	130.48	121.23	179.57	97.15	124.51
	1.25	92.70	78.25	100.54	109.04	121.31	151.81	97.50	102.80
0.0161	0.25	59.57	263.20	82.05	398.04	97.94	493.30	74.81	354.62
	0.5	63.15	161.67	83.11	243.11	97.96	303.68	75.11	210.49
	0.75	65.90	121.61	84.12	181.97	97.98	227.87	75.44	153.19
	1.0	68.08	100.17	85.07	149.37	98.01	186.89	75.78	122.48
	1.25	69.84	84.98	85.88	126.85	98.06	158.66	76.16	101.47
0.0214	0.25	45.98	276.34	73.74	475.37	81.98	538.81	60.25	371.49
	0.5	48.84	173.73	74.87	289.75	82.00	326.38	60.53	216.12
	0.75	51.04	132.04	75.94	220.28	82.01	245.57	60.84	157.45
	1.0	52.79	109.23	76.91	179.66	82.03	198.05	61.18	123.21
	1.25	54.21	92.91	77.72	154.14	82.06	168.14	61.55	101.94

Table 7. Theoretical predictions of collector efficiency improvements and further collector efficiency enhancements with $I_0 = 1100 \text{ W/m}^2$.

$\dot{m}(\text{kg s}^{-1})$	R	Type A		Type B		Type C		Type D	
		$I_{C,A}$	$E_{C,A}$	$I_{C,B}$	$E_{C,B}$	$I_{C,C}$	$E_{C,C}$	$I_{C,D}$	$E_{C,D}$
0.0107	0.25	91.63	264.23	107.11	328.13	133.44	432.37	104.32	317.08
	0.5	96.58	171.11	108.15	209.90	133.48	281.82	104.64	199.95
	0.75	100.37	134.35	109.14	158.99	133.53	216.32	104.97	149.18
	1.0	103.35	112.74	110.07	130.56	133.59	179.38	105.32	120.70
	1.25	105.74	97.25	110.89	110.47	133.69	153.36	105.69	100.70
0.0161	0.25	68.68	266.83	89.57	373.38	106.95	464.23	80.27	324.78
	0.5	72.47	177.05	90.66	238.26	106.97	298.43	80.58	201.04
	0.75	75.38	138.36	91.73	184.49	107.00	231.34	80.91	151.32
	1.0	77.69	116.61	92.71	153.33	107.03	192.06	81.27	122.42
	1.25	79.55	100.79	93.55	131.54	107.08	164.66	81.66	102.42
0.0214	0.25	54.03	270.11	80.58	448.67	89.92	511.46	64.94	343.52
	0.5	57.05	170.77	81.75	285.98	89.93	324.15	65.24	208.98
	0.75	59.38	131.68	82.86	221.78	89.94	248.97	65.56	155.39
	1.0	61.23	107.74	83.87	183.33	89.97	203.69	65.91	123.36
	1.25	62.72	93.85	84.72	160.74	89.99	176.80	66.29	104.69

Furthermore, the influences of inlet air temperatures on the collector efficiency and collector efficiency improvements for $I_0 = 1100 \text{ W/m}^2$ and $\dot{m} = 0.0214 \text{ kg/s}$ are illustrated with the recycle ratio and air mass flow rate parameters in Table 8 for comparison. The theoretical prediction shows that the collector efficiency declines with the decreasing inlet air temperature, whereas the collector efficiency improves with the increasing inlet air temperature.

Table 8. Theoretical predictions of collector efficiency and collector efficiency improvement for $I_0 = 1100 \text{ W/m}^2$ and $\dot{m} = 0.0214 \text{ kg/s}$.

$T_i(\text{K})$	R	Type A		Type B		Type C		Type D	
		$\eta_{C,A}$	$I_{C,A}$	$\eta_{C,B}$	$I_{C,B}$	$\eta_{C,C}$	$I_{C,C}$	$\eta_{C,D}$	$I_{C,D}$
293	0.25	0.633	54.03	0.742	80.58	0.781	89.92	0.678	64.94
	0.5	0.646	57.05	0.747	81.75	0.781	89.93	0.679	65.24
	0.75	0.655	59.38	0.752	82.86	0.781	89.94	0.681	65.56
	1.0	0.663	61.23	0.756	83.87	0.781	89.97	0.682	65.91
	1.25	0.669	62.72	0.759	84.72	0.781	89.99	0.684	66.29
303	0.25	0.629	60.47	0.739	88.57	0.777	98.18	0.676	72.42
	0.5	0.641	63.43	0.744	89.69	0.777	98.19	0.677	72.71
	0.75	0.650	65.70	0.748	90.74	0.777	98.21	0.678	73.02
	1.0	0.657	67.50	0.752	91.68	0.777	98.23	0.680	73.35
	1.25	0.662	68.95	0.755	92.44	0.777	98.25	0.681	73.72
313	0.25	0.625	65.77	0.736	95.18	0.773	105.07	0.674	78.75
	0.5	0.636	68.63	0.740	96.21	0.773	105.08	0.675	79.02
	0.75	0.644	70.82	0.744	97.18	0.773	105.09	0.676	79.32
	1.0	0.651	72.54	0.747	98.02	0.773	105.11	0.677	79.64
	1.25	0.656	73.92	0.748	98.29	0.774	105.14	0.679	79.98

5. Results and Discussion

The theoretical formulation of the current work helped to complete the understanding of the heat transfer behaviors by considering the comparisons among recycling double-pass operations of this study. In this section, the theoretical predictions and experimental results of external-recycle Types A [33], B, C and D are presented. The qualitative and quantitative graphs and tables display evaluations of the optimal efficient types. The best design involved a cross-corrugated absorber plate and bottom plate; both theoretical predictions and experimental results are discussed. This indicates that the proposed cross-corrugated solar air collectors and the thermal function are considerably improved. Meanwhile, the forced convective heat-transfer coefficient increases with the air mass flow rate for a given recycle ratio. Thus, it reaches a higher collector efficiency improvement, but further collector efficiency enhancements result in an inverse effect, as demonstrated in Tables 6 and 7. Operations of cross-corrugated solar air collectors with external recycling include considerations of both laminar-flow and turbulent-flow behaviors with the average Nusselt number (Equations (28)–(30)) and the Fanning friction factor (Equations (41)–(43)); the appropriate expressions were used to calculate the heat transfer rate and power consumption for both flow characteristics. In the present study, external recycling with air recirculation produced an effect of remixing inlet air with hot outgoing air, increasing the fluid velocity and convective heat-transfer coefficients as well. The concept of designing recycling solar air collectors involves the air circulation being heated twice in two subchannels before exiting the collector. The energy penalty with increasing friction loss must be taken into account, because the power requirements also increase [12]. This study proposes an optimal design of the recycling double-pass cross-corrugated device which is expected to consider the compensation between collector efficiency improvement $I_{C,i}$ ($i = A, B, C, D$). ($i = A, B, C, D$) due to external recycling and the power consumption increment $I_{P,i}$, due to pumping the air circulation into the two divided subchannels by embedding both the wavelike absorber plate and bottom plate.

A novel design for solar air collectors in raising the turbulence intensity by implementing a cross-corrugated absorber and bottom plates in parallel into the flat-plate conduit to conduct double-pass operation has been studied theoretically and experimentally. The multiplied effects of turbulent flow channels of solar air collector were examined to enhance the thermal performance, because both the wavelike absorber plate and bottom plate significantly induced vortices. Comparing the ratio of $I_{C,i}/I_{P,i}$ to those of the single-pass and flat-plate double-pass device with air mass flow rate and recycle ratio as parameters,

both the effects of external recycling and cross-corrugated plates enhanced the collector thermal efficiency in this study, as shown in Figures 13–15. The operation of recycling cross-corrugated solar air collectors offers a low-cost strategy in considerably enhancing the collector efficiency. The evaluation of a higher ratio of the collector efficiency improvements, $I_{C,A}$, $I_{C,B}$, $I_{C,C}$ and $I_{C,D}$, and the power consumption increments $I_{P,A}$, $I_{P,B}$, $I_{P,C}$ and $I_{P,D}$ for cross-corrugated double-pass solar air collectors resulted in suitable selection of the optimal design and led to economic benefits. The results indicated that the turbulent intensity increments when employing the cross-corrugated solar air collector could compensate for the power consumption increments with considerations of the economic feasibility, as represented graphically in Figures 13–15 for various air mass flow rates.

The air flow in double-pass flat-plate solar air collectors indicates a smooth-surface flow pattern in parallel conduits, which is the conventional and simplest geometry of the solar air collector associated with both a relatively low heat transfer rate and friction loss (i.e., $I_d/I_{P,d}$). The corrugated absorber plate represents more bearings from the eddy promotion accompanied by the advantage of heat transfer augmentation. The ratios of $I_{C,A}/I_{P,A}$, $I_{C,B}/I_{P,B}$, $I_{C,C}/I_{P,C}$ and $I_{C,D}/I_{P,D}$ reached an optimal recycling ratio for all air mass flow rates, e.g., $R = 0.5$, which symbolizes the lowest value of a power consumption increment in contrast to its highest collector efficiency improvement, and moves away from $R = 0.5$ due to either the larger power consumption increment for $R > 0.5$ or the smaller collector efficiency improvement for $R < 0.5$. All the ratios of $I_{C,A}/I_{P,A}$, $I_{C,B}/I_{P,B}$, $I_{C,C}/I_{P,C}$, $I_{C,D}/I_{P,D}$ and $I_d/I_{P,d}$ increased with the air mass flow rate. The largest increment in collector efficiency was attributed to Type C, which was the most efficient configuration cross-corrugated solar air collector, especially at lower air mass flow rates. Meanwhile, the power consumption increments of all external-recycle types were not much different from each other, except for Type D, which was due to equal recycling air mass flow rates $\dot{m}(R + 1)$ in both channels. Thus, the ratios of $I_{C,A}/I_{P,A}$, $I_{C,B}/I_{P,B}$, $I_{C,C}/I_{P,C}$ and $I_{C,D}/I_{P,D}$ were relative low under Type D in general. Furthermore, the lowest collector efficiency improvements were found to take place when employing Type A [33], as shown in Table 4, and resulted in a less thermally efficient configuration among all the proposed external-recycle configurations.

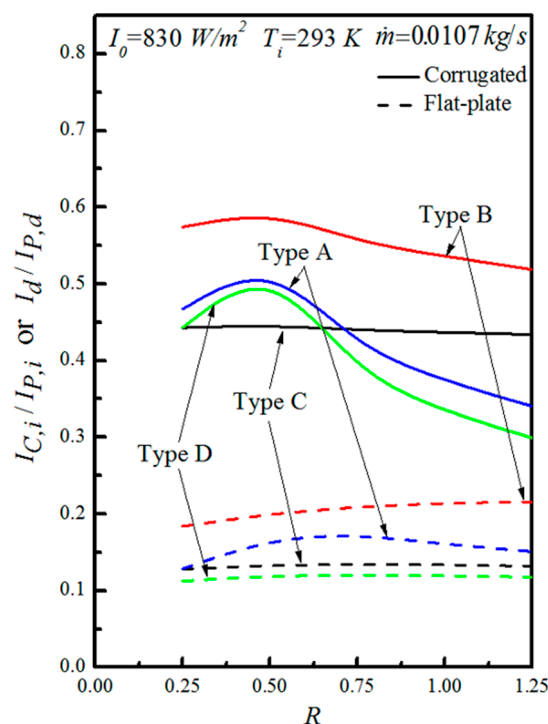


Figure 13. The ratio of the collector efficiency improvements and power consumption increments ($\dot{m} = 0.0107 \text{ kg/s}$).

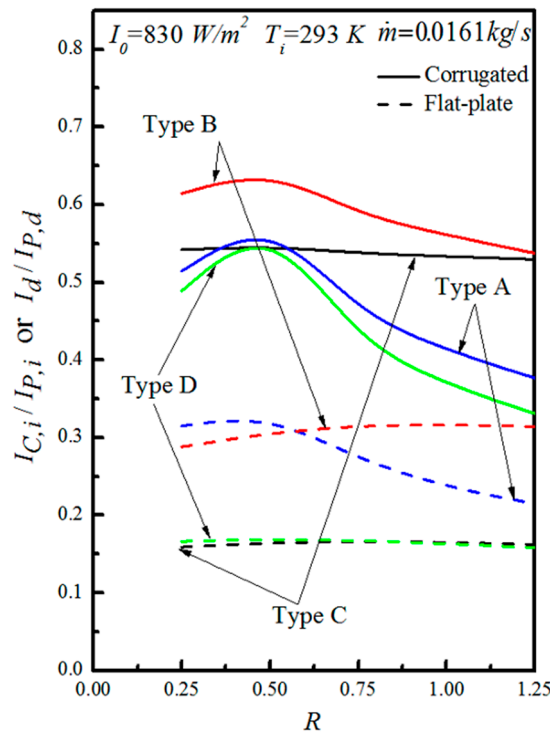


Figure 14. The ratio of the collector efficiency improvements and power consumption increments ($\dot{m} = 0.0161$ kg/s).

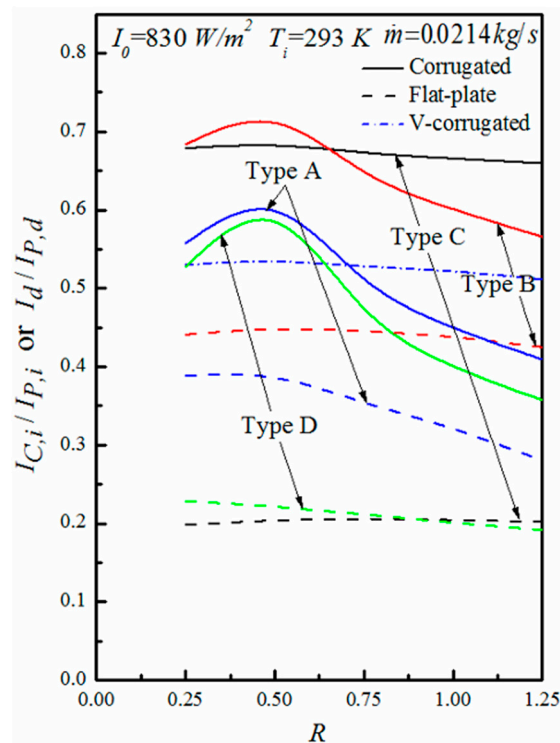


Figure 15. The ratio of the collector efficiency improvements and power consumption increments ($\dot{m} = 0.0214$ kg/s).

In addition, the substantial increase in the power consumption by raising the recycle ratio intensified the turbulence magnitude. The higher ratios of $I_{C,A}/I_{P,A}$, $I_{C,B}/I_{P,B}$, $I_{C,C}/I_{P,C}$ and $I_{C,D}/I_P$ denote the extent of collector efficiency improvements of double-pass cross-

corrugated solar air collectors, which were more significant than that of the double-pass flat-plate solar air collector compensating the energy consumption. The graphs depict significant differences in the trend for the ratios of the collector efficiency improvements and power consumption increments between Type C and the other types. However, the denominator of power consumption increment for Type C showed no extensive discrepancy on the recycling ratio, whereas the profiles of the ratios among Types A, B and D revealed insignificant variation. It is evident that the cross-corrugated double-pass solar air collector delivers greater economic and technical feasibility due to a greater and useful energy gain, albeit at the expense of a reduced amount of power consumption, as shown in Figures 13–15. The extents of collector efficiency improvements were more significant with the recycle ratios than those in the V-corrugated device of the same operational conditions [41]; thus, a higher value of $I_{C,A}/I_{P,A}$ is obtained by operating double-pass cross-corrugated solar air collectors with external recycling, as demonstrated in Figure 15. With those comparisons, the advantage of the cross-corrugated design for solar air collectors is evident. The present work is actually the extension of our previous work [33] except for using more types of various external-recycle operations instead of Type A [33]. It implies that, under all air mass flow rates and recycle ratios, various external-recycle operations of Type B, Type C and Type D are better for improving the collector efficiency than that of Type A [33], as shown in Figure 15. A suitable selection of the operating parameters for the recycling double-pass cross-corrugated solar air collectors would be regarded as an evident decision for realizing both practical and beneficial applications.

6. Conclusions

Theoretical and experimental studies on the thermal performance of four proposed configurations for recycling cross-corrugated double-pass solar air collectors used to increase heat transfer efficiency have been introduced, considering the hydraulic dissipated energy increments. They were designed by implementing both transverse sinusoidal corrugated absorbers and bottom plates to strengthen the forced convective heat-transfer coefficient, which produced about a 540% increment in further collector efficiency enhancements compared to the flat-plate solar air collector, as shown in Tables 7 and 8. Additionally, it has created a threefold greater ratio the collector efficiency improvement and power consumption increment, as presented in Figures 13–15. Operating these four external-recycle types with a smaller recycle ratio, i.e., $R = 0.5$, leads to better device performance due to the augmented turbulence intensity and enlarged heat transfer area coupled with a relatively small loss in friction, which is expressed in terms of the ratio of the collector efficiency improvement and power consumption increment compared to the economic consideration, in terms of $I_{C,A}/I_{P,A}$, $I_{C,B}/I_{P,B}$, $I_{C,C}/I_{P,C}$ and $I_{C,D}/I_P$, which is confirmed in Figures 13–15.

This study corroborates the acceptable thermal performance of the proposed various external-recycle configurations of cross-corrugated solar air collectors by performing comparisons with conventional solar air heaters in previous studies. In this theoretical and experimental study, a recycling double-pass solar air collector was examined in four configurations with external recycling under various operational conditions. The results are summarized into the following conclusive findings:

- (1) The Type C external-recycle configuration is the most efficient design compared to the other types;
- (2) The economic feasibility analysis suggested the optimal operating conditions at $R = 0.5$ for compensating a relatively low hydraulic dissipated energy increment;
- (3) Applications of the recycling double-pass cross-corrugated solar air collector are technically practical under a higher collector thermal efficiency when compared to the flat-plate solar air collector;
- (4) Both the collector efficiency and collector efficiency of cross-corrugated solar air collectors improves with the increasing recycling ratio, air mass flow rate and incident solar radiation, but declines with decreasing inlet air temperature;

- (5) Deviations in the accuracy of the theoretical predictions in the collected data from experimentation are larger under higher air mass flow rates;
- (6) The advantage of the present design is evident: a Type C external-recycle configuration would be best recommended for accomplishing optimal selection from an economic efficiency standpoint.

Author Contributions: This paper is a result of the full collaboration of all the authors. C.-D.H., Conceptualization; H.C., Writing—original draft; C.-F.H., Data curation; Y.-C.L., Validation. All authors have read and agreed to the published version of the manuscript.

Funding: This research received no external funding.

Acknowledgments: The authors wish to thank the Ministry of Science and Technology of the Republic of China (Taiwan) and Tamkang University for their financial support.

Conflicts of Interest: The authors declare no conflict of interest.

Nomenclature

A_c	surface area of the collector (m^2)
B_i	coefficients, $i = 1, 2, \dots, 6$
C_i	coefficients, $i = 1, 2$
C_p	specific heat of air at constant pressure (J/kgK)
De_0	equivalent hydraulic diameter of the single-pass device (m)
De_a	equivalent hydraulic diameter of the lower channel of double-pass device (m)
De_b	equivalent hydraulic diameter of the upper channel of double-pass device (m)
Er	deviation of the experimental measurements from theoretical predictions
$E_{C,i}$	further enhancement in collector efficiency, $i = A, B, C, D$
f_F	Fanning friction factor
F_i	coefficients, $i = 1, 2, 3$
G_i	coefficients, $i = 1, 2, \dots, 7$
H_c	average channel thickness of the inner cover and the absorber plate (m)
H_g	average channel gap between the absorber plate and the bottom plate (m)
h_0	convection coefficient in the single-pass device (W/m^2K)
h_a	convection coefficient between the bottom and lower channel (W/m^2K)
h'_a	convection coefficient between the absorber plate and lower channel (W/m^2K)
h_b	convection coefficient between the absorber plate and upper channel (W/m^2K)
h'_b	convection coefficient between the inner cover and upper channel (W/m^2K)
h_{c1-c2}	convective coefficient between two glass covers (W/m^2K)
$h_{r,c1-c2}$	radiation coefficient between two glass covers (W/m^2K)
$h_{r,c2-s}$	radiation coefficient from the outer cover to the ambient (W/m^2K)
$h_{r,p-c1}$	radiation coefficient between the inner cover and absorber plate (W/m^2K)
$h_{r,p-R}$	radiation coefficient between absorber plate and bottom plate (W/m^2K)
h_w	convective coefficient for air flowing over the outer cover (W/m^2K)
I_0	incident solar radiation (W/m^2)
I_i	coefficients, $i = 1, 2$
$I_{p,i}$	percentage of power consumption increments, $i = A, B, C, D$
$I_{C,i}$	percentage of collector efficiency improvements in corrugated type, $i = A, B, C, D$
I_d	percentage of collector efficiency improvements in flat-plate type
k	thermal conductivity of the air (W/mK)
L	channel length (m)
$\ell W_{f,a}$	lower channel friction loss of double-pass device (J/kg)
$\ell W_{f,b}$	upper channel friction loss of double-pass device (J/kg)
$\ell W_{f,s}$	friction loss of downward-type single-pass device (J/kg)
$M_{a,i}$	air mass flow rate in the lower channel (kg/s), $i = A, B, C, D$
$M_{b,i}$	air mass flow rate in the upper channel (kg/s), $i = A, B, C, D$
\dot{m}	air mass flow rate (kg/s)
N_{exp}	number of the experimental measurements
Nu_0	Nusselt number in the flat-plate collector

Nu_a	Nusselt number in the lower channel
Nu_b	Nusselt number in the upper channel
$P_{C,i}$	power consumption for the cross-corrugated solar air collector (W), $i = A, B, C, D$
$P_{C,d}$	power consumption for the double-pass flat-plate solar air collector (W)
Q_u	useful energy gain by flowing air (W)
R	recycle ratio
Ra	Rayleigh number
Re_0	Reynolds number in the flat-plate collector
Re_a	Reynolds number in the lower channel
Re_b	Reynolds number in the upper channel
$S_{\eta_{exp}}$	experimental uncertainty of an individual measurement
$\overline{S_{\eta_{exp}}}$	mean value of $S_{\eta_{exp}}$
$T_a(z)$	axial fluid temperature distribution in the lower channel (K)
$T_b(z)$	axial fluid temperature distribution in the upper channel (K)
$T_a(\xi)$	dimensionless axial temperature distribution in the lower channel (K)
$T_b(\xi)$	dimensionless axial temperature distribution in the upper channel (K)
$T_{a,0}$	mixing temperature of the lower channel at $x = 0$ (K)
$T_{a,L}$	outlet temperature of the lower channel (K)
$T_{b,0}$	temperature of the upper channel b at $x = 0$ (K)
$T_{b,L}$	temperature of the upper channel at $x = L$ (K)
$T_{a,m}$	average temperature of the lower channel (K)
$T_{b,m}$	average temperature of the upper channel (K)
T_{c1}	temperature of the inner glass cover (K)
T_{c2}	temperature of the outer glass cover (K)
$T_{c1,m}$	average temperature of the inner glass cover (K)
$T_{c2,m}$	average temperature of the outer glass cover (K)
T_i	inlet temperature of the lower channel (K)
T_p	temperature of the corrugated absorber plate (K)
$T_{p,m}$	average temperature of the corrugated absorber plate (K)
T_R	temperature of the bottom plate (K)
T_s	ambient temperature (K)
U_B	loss coefficient from the bottom plate to the environment (W/m ² K)
U_{B-s}	loss coefficient from the surfaces of edges and bottom to the environment (W/m ² K)
U_{c1-s}	loss coefficient from the inner cover to the environment (W/m ² K)
U_L	overall loss coefficient (W/m ² K)
U_T	loss coefficient from the top to the environment (W/m ² K)
$\overline{v_0}$	average velocity of the single-pass device (m/s)
$\overline{v_a}$	average velocity of the lower channel (m/s)
$\overline{v_b}$	average velocity of the upper channel (m/s)
Y_i	coefficient, $i = 1, 2$
W	collector width (m)
z	axial coordinate along the flow direction (m)
Greek Letters	
α_p	absorptivity of the absorber plate
β	thermal expansion coefficient (1/K)
η_C	collector efficiency of the cross-corrugated solar air heater
η_D	collector efficiency of the double-pass flat-plate
η_S	collector efficiency of the downward-type single-pass device
$\eta_{exp,i}$	experimental data of collector efficiency
$\overline{\eta_{exp,i}}$	mean value of the experimental data $\eta_{exp,i}$
$\eta_{theo,i}$	theoretical prediction of collector efficiency
τ_g	transmittance of glass cover
ε_g	emissivity of the glass cover
ε_p	emissivity of the absorber plate
ρ	air density (kg/m ³)
μ	air viscosity (kg/s m)
σ	Stefan–Boltzmann constant ($=5.682 \times 10^{-8}$) (W/m ² K ⁴)
ξ	dimensionless channel position

References

1. Kumar, L.; Hasanuzzaman, M.; Rahim, N.A. Global advancement of solar thermal energy technologies for industrial process heat and its future prospects: A review. *Energy Convers. Manag.* **2019**, *195*, 885–908. [[CrossRef](#)]
2. Seluck, M.K. *Solar Air Heaters and Their Applications*; Sayigh, A.A.M., Ed.; Academic Press: New York, NY, USA, 1977.
3. Chen, X.; Yang, H.; Lu, L.; Wang, J.; Liu, W. Experimental studies on a ground coupled heat pump with solar thermal collectors for space heating. *Energy* **2011**, *36*, 5292–5300.
4. Design, S.S. Experimental investigation and analysis of a solar drying system. *Energy Convers. Manag.* **2013**, *8*, 27–34.
5. Bari, E.; Noel, J.Y.; Comini, G.; Cortella, G. Air-cooled condensing systems for home and industrial appliances. *Appl. Therm. Eng.* **2005**, *25*, 1446–1458. [[CrossRef](#)]
6. Razika, I.; Nabila, I.; Madani, B.; Zohra, H.F. The effects of volumetric flow rate and inclination angle on the performance of a solar thermal collector. *Energy Convers. Manag.* **2014**, *78*, 931–937. [[CrossRef](#)]
7. Al-Kayiem, H.H.; Yassen, T.A. On the natural convection heat transfer in a rectangular passage solar air heater. *Sol. Energy* **2015**, *12*, 10–18. [[CrossRef](#)]
8. Das, B.; Mondol, J.D.; Negi, S.; Smyth, M.; Pugsley, A. An experiment was conducted to investigate the performance of a novel sand coated and sand filled (SCSF) polycarbonate sheet based solar air collector (SAC) under controlled indoor conditions with variable air flow rates and solar inputs. *Renew. Energy* **2021**, *164*, 990–1004. [[CrossRef](#)]
9. El-Sebaei, A.A.; Shalaby, S.M. Experimental investigation of an indirect-mode forced convection solar dryer for drying thymus and mint. *Energy Convers. Manag.* **2013**, *74*, 109–116. [[CrossRef](#)]
10. Vaziri, R.; Ilkan, M.; Egelioglu, F. Experimental performance of performance of perforated glazed solar air heaters and un-glazed transpired solar air heater. *Sol. Energy* **2015**, *119*, 251–260. [[CrossRef](#)]
11. Fudholi, A.; Sopian, K.; Othman, M.Y.; Ruslan, M.H.; Bakhtyar, B. Energy analysis and improvement potential of finned double-pass solar collector. *Energy Convers. Manag.* **2013**, *75*, 234–240. [[CrossRef](#)]
12. Gupta, M.K.; Kaushik, S.C. Performance evaluation of solar air heater for various artificial roughness geometries based on energy, effective and exergy efficiencies. *Renew. Energy* **2009**, *34*, 465–476. [[CrossRef](#)]
13. Singh, S.; Dhiman, P. Thermal performance of double pass packed bed solar air heaters—A comprehensive review. *Renew. Sustain. Energy Rev.* **2016**, *53*, 1010–1031. [[CrossRef](#)]
14. Ravi, R.K.; Saini, R.P. A review on different techniques used for performance enhancement of double pass solar air heaters. *Renew. Sustain. Energy Rev.* **2016**, *56*, 941–952. [[CrossRef](#)]
15. Karim, M.A.; Perez, E.; Amin, Z.M. Mathematical modelling of counter flow v-groove solar air collector. *Renew. Energy* **2014**, *67*, 192–201. [[CrossRef](#)]
16. Hosseini, S.S.; Ramiar, A.; Ranjbar, A.A. Numerical investigation of natural convection solar air heater with different fins shape. *Renew. Energy* **2018**, *117*, 488–500. [[CrossRef](#)]
17. Sharma, K.S.; Kalamkar, V.R. Experimental and numerical investigation of forced convection heat transfer in solar air heater with thin ribs. *Sol. Energy* **2017**, *147*, 227–291. [[CrossRef](#)]
18. Skullong, S.; Promvong, P.; Thianpong, C.; Pimsarn, M. Thermal performance in solar air heater channel with combined wavy-groove and perforated-delta wing vortex generators. *Sol. Appl. Eng.* **2016**, *100*, 611–620. [[CrossRef](#)]
19. Tamna, S.; Skullong, S.; Thianpong, C.; Promvong, P. Heat transfer behaviors in a solar air heater channel with multiple V-baffle vortex generators. *Sol. Energy* **2014**, *110*, 720–735. [[CrossRef](#)]
20. Mohammadi, K.; Sabzpooshani, M. Appraising the performance of a baffled solar air heater with external recycle. *Energy Convers. Manag.* **2014**, *88*, 239–250. [[CrossRef](#)]
21. Saini, R.P.; Singal, S.K. A review on roughness geometry used in solar air heaters. *Sol. Energy* **2007**, *81*, 1340–1350.
22. Nowzari, R.; Aldabbagh, L.B.Y.; Egelioglu, F. Single and double pass solar air heaters with partially perforated cover and packed mesh. *Energy* **2014**, *73*, 694–702. [[CrossRef](#)]
23. Languri, E.M.; Taherian, H.; Hooman, K.; Reisel, J. Enhanced double-pass solar air heater with and without porous medium. *Int. J. Green Energy* **2011**, *8*, 643–654. [[CrossRef](#)]
24. Ho, C.D.; Lin, C.S.; Chuang, Y.C.; Chao, C.C. Performance of wire mesh packed double-pass solar air heaters with external recycle. *Renew. Energy* **2013**, *57*, 479–489. [[CrossRef](#)]
25. El-Sebaei, A.A.; Aboul-Enein, S.; Ramadan, M.R.I.; Shalaby, S.M.; Moharram, B.M. Investigation of thermal performance of double-pass flat and v-corrugated plate solar air heaters. *Energy* **2011**, *36*, 1076–1086. [[CrossRef](#)]
26. Ho, C.D.; Chang, H.; Hong, Z.S.; Huang, C.C.; Chen, Y.H. Increasing the Device Performance of Recycling Double-Pass W-ribs Solar Air Heaters. *Energies* **2020**, *13*, 2133. [[CrossRef](#)]
27. Satcunanathan, S.; Deonarine, S. A two pass solar air heater. *Sol. Energy* **1973**, *15*, 41–49.
28. Wijesundera, N.E.; Ah, L.L.; Tjioe, L.E. Thermal performance study of two-pass solar air heaters. *Sol. Energy* **1982**, *28*, 363–370. [[CrossRef](#)]
29. Naphon, P. Heat transfer characteristics and pressure drop in channel with V corrugated upper and lower plates. *Energy Convers. Manag.* **2007**, *48*, 1516–1524. [[CrossRef](#)]
30. Qin, Y.; Guan, X.; Dun, Z.; Liu, H. Numerical simulation on fluid flow and heat transfer in a corrugated plate air preheater. *J. Chin. Soc. Power Eng.* **2015**, *35*, 213–218.

31. Dhiman, P.; Singh, S. Thermal performance assessment of recyclic double-pass flat and V-corrugated plate solar air heaters. *Int. J. Sustain. Energy* **2015**, *36*, 1–23. [[CrossRef](#)]
32. Muley, A.; Manglik, R.M. Experimental study of turbulent flow heat transfer and pressure drop in a plate heat exchanger with chevron plates. *J. Heat Transf.* **1999**, *121*, 110–117. [[CrossRef](#)]
33. Ho, C.D.; Chang, H.; Hsiao, C.F.; Huang, C.C. Device performance improvement of recycling double-pass cross-corrugated solar air collectors. *Energies* **2018**, *11*, 338–350.
34. Duffie, J.A.; Beckman, W.A. *Solar Engineering of Thermal Processes*; Wiley: New York, NY, USA, 1980.
35. Klein, S.A. Calculation of monthly average transmittance-absorptance product. *Sol. Energy* **1979**, *23*, 547–551. [[CrossRef](#)]
36. Piao, Y.; Hauptmann, E.G.; Iqbal, M. Forced convective heat transfer in cross-corrugated solar air heaters. *J. Sol. Energy Eng.* **1994**, *116*, 212–214. [[CrossRef](#)]
37. Lin, W.X.; Gao, W.F.; Liu, T. A parametric study of the thermal performance of cross-corrugated solar air collectors. *Appl. Eng.* **2006**, *26*, 1043–1053. [[CrossRef](#)]
38. Heaton, H.S.; Reynolds, W.C.; Kays, W.M. Heat transfer in annular passages. simultaneous development of velocity and temperature fields in laminar flow. *Int. J. Heat Mass Transf.* **1964**, *7*, 763–781. [[CrossRef](#)]
39. Zhang, L.Z. Numerical study of periodically fully developed flow and heat transfer in cross-corrugated triangular channels in transitional flow regime. *Numer. Heat Transf. Part A* **2005**, *48*, 387–405. [[CrossRef](#)]
40. Moffat, R.J. Describing the uncertainties in experimental results. *Exp. Therm. Fluid Sci.* **1988**, *1*, 3–17. [[CrossRef](#)]
41. Ho, C.D.; Hsiao, C.F.; Chang, H.; Hsiao, C.F.; Tien, Y.E.; Hong, Z.S. Efficiency of recycling double-pass V-corrugated solar air collectors. *Energies* **2018**, *10*, 875–889.